

Quasi-elastic scattering and transfer angular distribution for $^{10,11}\text{B} + ^{232}\text{Th}$ systems at near-barrier energies

Shradha Dubey,^{1,2,*} D. C. Biswas,^{1,†} S. Mukherjee,² D. Patel,^{2,‡} Y. K. Gupta,¹ G. K. Prajapati,¹ B. N. Joshi,¹ L. S. Danu,¹ S. Mukhopadhyay,¹ B. V. John,¹ S. V. Suryanarayana,¹ and R. P. Vind¹

¹Nuclear Physics Division, Bhabha Atomic Research Centre, Mumbai 400085, India

²Physics Department, Faculty of Science, M.S. University of Baroda, Vadodra 390002, India

(Received 31 March 2016; revised manuscript received 16 September 2016; published 14 December 2016)

Quasi-elastic scattering and transfer angular distributions for $^{10,11}\text{B} + ^{232}\text{Th}$ reactions have been measured simultaneously in a wide range of bombarding energies around the Coulomb barrier. The quasi-elastic angular distribution data are analyzed using the optical model code ECIS with phenomenological Woods-Saxon potentials. The obtained potential parameters suggest the presence of usual threshold anomaly, confirming tightly bound characteristics for both the projectiles. The reaction cross sections are obtained from the fitting of quasi-elastic angular distribution data. The reduced cross sections at sub-barrier energies compared with $^6\text{Li} + ^{232}\text{Th}$ systems show a systematic dependence on projectile breakup energy. The angular distribution of the transfer products show similar behavior for both the systems.

DOI: [10.1103/PhysRevC.94.064610](https://doi.org/10.1103/PhysRevC.94.064610)

I. INTRODUCTION

In heavy ion reactions, the interplay between the intrinsic structure and the reaction dynamics of the interacting nuclei is very important at energies near the Coulomb barrier. The study of elastic scattering and transfer processes in these reactions provides rich information on various reaction channel couplings. Several aspects of heavy ion reactions have been investigated over recent decades from the analysis of elastic scattering data using different optical model codes. One of the most important features of the heavy ion elastic scattering at energies close to the Coulomb barrier is the peculiar behavior of the optical potential, known as the threshold anomaly (TA) [1]. The real and imaginary optical potential parameters vary strongly at beam energies below the Coulomb barrier. The rapid decrease of the imaginary part of the optical potential below the barrier leads to a local peak in real part and this behavior can be understood using a dispersion relation between the real and the imaginary parts of the optical potential [1–4]:

$$\Delta V(E) = \frac{P}{\pi} \int_{-\infty}^{+\infty} \frac{W(E')}{E' - E} dE'. \quad (1)$$

Also,

$$V(E) = V_o + \Delta V(E), \quad (2)$$

where P is the principal value of the integral, $V(E)$ is dynamical real potential, and ΔV is dynamical polarization potential. Here, V_o is independent of energy and $W(E)$ is the energy-dependent imaginary potential.

The threshold anomaly phenomena have been studied extensively in heavy ion reactions involving either weakly or tightly bound projectiles [4–15]. For weakly bound projectiles, breakup threshold anomaly (BTA) has been observed, where

a repulsive polarization potential is generated due to the coupling of breakup channels to the elastic scattering, which causes an increase in the imaginary potential and corresponding decrease in the real part [16–18]. We have reported earlier the presence of BTA in the case of the $^6\text{Li} + ^{232}\text{Th}$ system. Although the breakup threshold for ^7Li (2.47 MeV) is not significantly larger than ^6Li (1.48 MeV), still $^7\text{Li} + ^{232}\text{Th}$ shows usual TA [19]. For the ^9Be projectile, the breakup threshold energy is 1.57 MeV and therefore it is expected to exhibit BTA. However, recently Camacho *et al.* have carried out a detailed analysis of the energy dependence of the optical potentials for the $^9\text{Be} + ^{208}\text{Pb}$, ^{209}Bi systems [20]. It is reported that the fusion imaginary potential indicates the presence of usual TA in these reactions, similar to that observed in tightly bound systems, but the direct reaction imaginary potential shows a BTA behavior.

There are very limited elastic scattering data for ^{10}B and ^{11}B projectiles with heavy targets [14, 15] and so far there have been no measurements reported for $^{10,11}\text{B} + ^{232}\text{Th}$ systems. The systematic investigation of the energy dependence of real and imaginary potentials for the $^{10,11}\text{B} + ^{232}\text{Th}$ systems is important to establish the presence of TA or BTA in these reactions. The use of the heavy target in the investigation of TA or BTA gives an advantage, as the effect is expected to be more pronounced due to large Coulomb effects. However, due to the presence of the low-lying excited states of the heavy targets, it is very difficult to separate the inelastic contributions from the elastic scattering data. In the past, optical model analysis have been carried out for quasi-elastic scattering data and it is reported that the inclusion of the inelastic channels with the elastic cross section have negligible effect on the extracted parameters [21, 22].

Comparison of different reaction quantities measured simultaneously in heavy ion reactions provides useful information on the reaction mechanism as well as structural aspects of the interacting nuclei. Among them, transfer processes significantly dominate at sub-barrier energies and influence the fusion cross section [23–26]. Since we can derive the reaction

*Corresponding author: shradha30686@gmail.com

†Corresponding author: dcbiswas@barc.gov.in

‡Present address: IMP-CAS, Lanzhou, China.

cross section from elastic scattering angular distribution analysis, it is important to investigate simultaneously the transfer processes to understand the role of projectile structure in heavy ion reaction dynamics.

In the present work, we have measured simultaneously the quasi-elastic (elastic + low-lying inelastic) scattering and transfer angular distributions for $^{10,11}\text{B} + ^{232}\text{Th}$ systems at energies from 10% below the Coulomb barrier ($V_b = 54.2$ MeV) to approximately 20% above the barrier to investigate the reaction mechanism. From the optical model analysis of the quasi-elastic angular distribution data, the potential parameters were determined to investigate the threshold anomaly for $^{10,11}\text{B} + ^{232}\text{Th}$ systems. The experimental details are given in Sec. II. The energy dependence of potential parameters and the dispersion relation analysis are discussed in Sec. III. The analysis of transfer as well as reaction cross sections for $^{10,11}\text{B} + ^{232}\text{Th}$ reactions are presented in Sec. IV. In Sec. V, a systematic study of reduced reaction cross section has been discussed. The summary and conclusions of the present work are presented in Sec. VI.

II. EXPERIMENTAL DETAILS

The quasi-elastic scattering and transfer angular distribution measurements were carried out using $^{10,11}\text{B}$ beams from the 14UD BARC-TIFR Pelletron facility, Mumbai, India, at energies $E_{\text{lab}} = 52, 53, 54, 55, 56, 57, 59, 61,$ and 65 MeV for the $^{11}\text{B} + ^{232}\text{Th}$ system and $49, 51, 52, 53, 54, 55, 56, 57, 59, 61,$ and 65 MeV for the $^{10}\text{B} + ^{232}\text{Th}$ system. The range of energies relative to the Coulomb barrier is ~ 0.96 to 1.20 for $^{11}\text{B} + ^{232}\text{Th}$ system and it is ~ 0.90 to 1.19 for the $^{10}\text{B} + ^{232}\text{Th}$ system. A self-supporting metallic foil of ^{232}Th with a thickness of 1.3 mg/cm² was used as target. Four silicon surface barrier detector telescopes with different thicknesses (T_1 with $\Delta E = 25$ μm and $E = 300$ μm ; T_2 , $\Delta E = 40$ μm and $E = 300$ μm ; T_3 , $\Delta E = 25$ μm and $E = 300$ μm ; and T_4 , $\Delta E = 25$ μm and $E = 300$ μm) were used to detect simultaneously the elastically scattered as well as projectile-like fragments. The detector telescopes were mounted on a movable arm at an angular separation of 10° inside a general-purpose scattering chamber. All four telescopes were mounted at a distance of 21.1 cm from the target, having a front collimator of 6 mm, which imposes an angular uncertainty of $\pm 0.81^\circ$. Two monitor detectors with thickness of around 300 μm were mounted at 65 cm from the target with 1 -mm collimator. They were kept at fixed angles of $\pm 18^\circ$ with respect to the beam direction, for absolute normalization and beam monitoring purposes. The angular distributions were measured in steps of 5° in the angular range from 35° to 170° . Figure 1 shows a typical two-dimensional scatter plot of the pulse heights of ΔE and E_{res} (residual energy) detectors for the $^{11}\text{B} + ^{232}\text{Th}$ system at $E_{\text{lab}} = 61$ MeV and $\theta_{\text{lab}} = 90^\circ$. The bounded region (dashed line) on $Z = 5$ are quasi-elastic events and the marked line width shown in the inset of Fig. 1 is used for the cross section calculation. As the width of the elastic peak is about 650 keV (FWHM), the low-lying excited states of ^{232}Th target (49.37 and 162.12 keV) could not be separated from the elastic peak in the present experimental technique. Thus, these inelastic contributions are included in quasi-elastic angular distribution data.

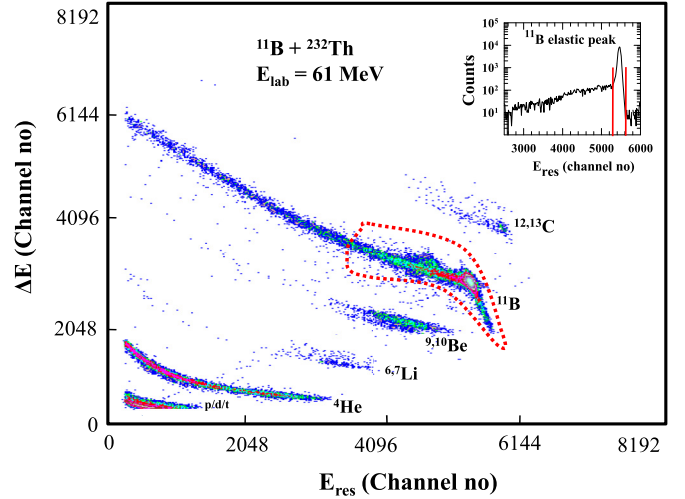


FIG. 1. A typical two-dimensional plot of ΔE versus E_{res} (residual energy) for the $^{11}\text{B} + ^{232}\text{Th}$ system at $E_{\text{lab}} = 61$ MeV and $\theta_{\text{lab}} = 90^\circ$. The bounded region (dashed line) on $Z = 5$ events shows quasi-elastic events and the inset in Fig. 1, shown by two vertical lines, indicates the data used for the optical model analysis.

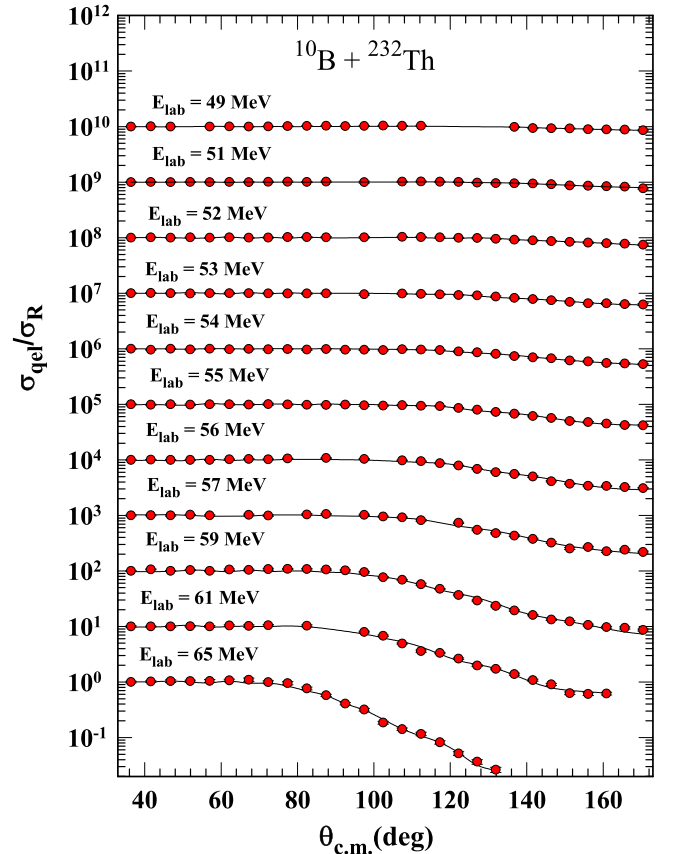


FIG. 2. Quasi-elastic (σ_{qel}) scattering angular distributions normalized with Rutherford cross section (σ_{R}) for the $^{10}\text{B} + ^{232}\text{Th}$ system at various energies after suitably scaling. The solid line represents the Wood-Saxon fit (see text).

TABLE I. Optical potential parameters and reaction cross sections (σ_R) of $^{10}\text{B} + ^{232}\text{Th}$ system obtained using ECIS code. The transfer cross sections (σ_{tr}) presented here are obtained by adding the measured cross sections for $^{12,13}\text{C}$, $^{9,10}\text{Be}$, and $^{6,7}\text{Li}$.

E_{lab} (MeV)	V_r (MeV)	V_i (MeV)	$\frac{\chi^2}{n}$	σ_R (mb)	σ_{tr} (mb)
49	492.4	6.49	0.87	6.24	2.23 ± 0.47
51	294.5	11.60	0.23	16.10	4.09 ± 0.68
52	218.2	18.63	0.26	38.73	6.06 ± 1.20
53	153.0	55.74	0.21	90.97	9.64 ± 1.17
54	132.8	55.99	0.84	121.81	13.61 ± 1.42
55	128.4	50.90	0.55	153.52	16.55 ± 1.30
56	120.8	49.50	4.35	197.20	21.61 ± 1.22
57	106.4	57.23	3.48	264.91	30.18 ± 2.40
59	83.47	86.76	5.84	451.72	41.95 ± 1.66
61	59.07	84.00	3.76	551.22	48.89 ± 1.65
65	77.85	92.62	2.43	824.50	54.81 ± 4.49

III. OPTICAL MODEL ANALYSIS OF QUASI-ELASTIC SCATTERING AND DISPERSION RELATION

The experimental quasi-elastic scattering cross sections measured at several energies are plotted as a function of $\theta_{c.m}$ after normalizing with the Rutherford cross section as shown

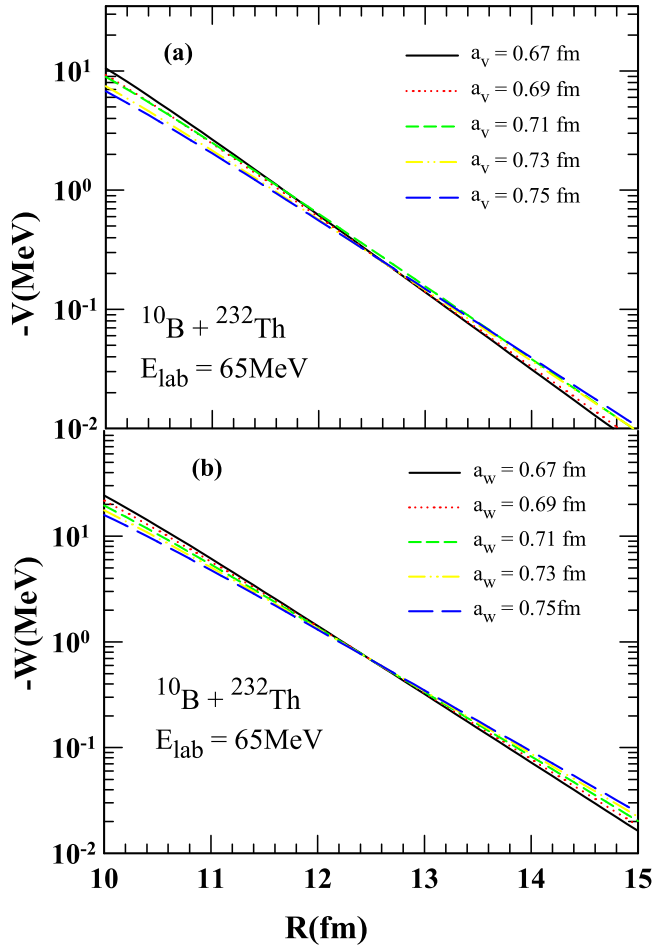


FIG. 3. Sensitivity radii based on the crossing of the real (a) and imaginary (b) parts of the WSP potential at $E_{lab} = 65$ MeV for different diffuseness parameter values (a_v and a_w).

TABLE II. Optical model parameters [28] and transfer (σ_{tr}) as well as reaction cross section (σ_R) values for the $^{11}\text{B} + ^{232}\text{Th}$ system at different energies.

E_{lab} (MeV)	V_r (MeV)	V_i (MeV)	$\frac{\chi^2}{n}$	σ_R (mb)	σ_{tr} (mb)
52	194.0	0.13	1.58	7.02	6.21 ± 0.56
53	149.2	15.03	0.64	29.81	8.39 ± 0.53
54	162.0	31.43	1.21	89.74	14.44 ± 0.93
55	134.2	27.32	4.06	105.40	16.09 ± 1.01
56	126.0	51.44	3.52	216.21	24.77 ± 1.35
57	109.4	57.02	4.70	279.72	35.75 ± 1.15
59	121.5	59.23	4.90	432.61	37.80 ± 2.16
61	73.67	89.30	11.2	601.70	38.79 ± 1.47
65	53.45	109.70	9.21	886.42	42.27 ± 1.48

in Fig. 2. The angular distribution data are analyzed by using a phenomenological Woods-Saxon form of potential (WSP). The optical model fits to the quasi-elastic scattering data are performed using the ECIS code [27]. The WSP is an optical potential that has been successfully used in a wide range of energies to describe a large variety of reactions including inelastic scattering, fusion excitation functions, and barrier distributions. In the fitting procedure, radius parameters were initially allowed to vary with fixed depths and diffuseness parameters for both the real and imaginary parts. The analysis of the data on the entire energy range yielded a value of $r_0 = 1.06$ fm and it was kept fixed throughout in searching the other parameters. A grid search was made on the diffuseness parameters, a_v (real) and a_w (imaginary) in the range of

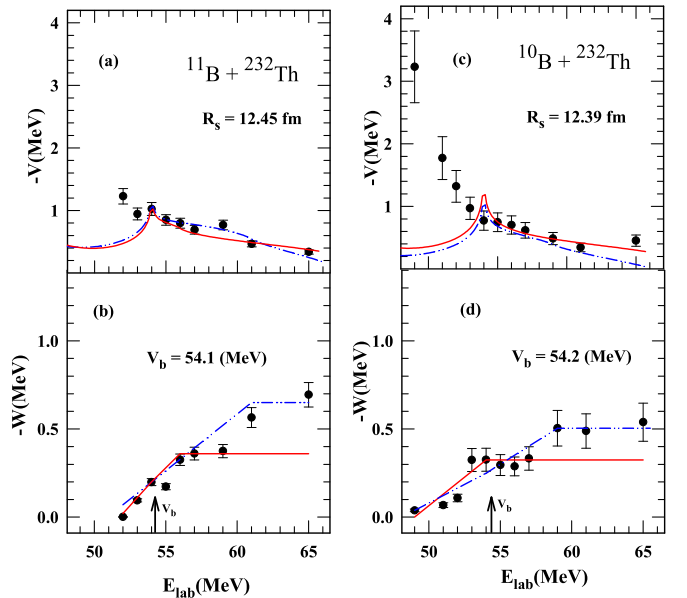


FIG. 4. Energy dependence of the real and imaginary potentials at sensitivity radii $R_s = 12.39$ fm for the $^{10}\text{B} + ^{232}\text{Th}$ system in panels (a) and (b) and at $R_s = 12.45$ fm for $^{11}\text{B} + ^{232}\text{Th}$ in panels (c) and (d). Solid (red) and dashed (blue) lines are two different sets of line-segment fits (see text). Arrows in the panels (b) and (d) indicate the positions of Coulomb barriers (V_b) for $^{11}\text{B} + ^{232}\text{Th}$ and $^{10}\text{B} + ^{232}\text{Th}$, respectively.

0.67 to 0.75 fm, in steps of 0.02 fm. For each diffuseness parameter, the potential depths, V_r (real) and V_i (imaginary), were varied to minimize χ^2 . The best-fit values were obtained to be $a_v = a_w = 0.71$ fm. Thus, radius (r_0) and diffuseness parameters for both real and imaginary parts were fixed to 1.06 and 0.71 fm, respectively for all the energies. The depths of the real and imaginary potentials were varied to obtain the minimum value of χ^2 . Typical best-fit calculations to the angular distributions are shown by solid lines in Fig. 2 for the $^{10}\text{B} + ^{232}\text{Th}$ system. The best-fitted potential parameters are shown in Table I for $^{10}\text{B} + ^{232}\text{Th}$ and in Table I $^{11}\text{B} + ^{232}\text{Th}$ systems [28].

The angular distribution and reaction cross section values are known to be sensitive to strong absorption radius. The crossover point where depths of the potential corresponding to different diffuseness parameters intersect (see Fig. 3) is referred to as radii of sensitivity [3,8,10,11,13,29]. The radii of sensitivity R_{sr} and R_{si} corresponding to the real and imaginary parts, respectively, were determined in the present

analysis. The radius parameters were kept fixed and the depth parameters of the real and imaginary parts were varied for each of the diffuseness parameters from 0.67 to 0.75 fm, in steps of 0.02 fm for all the energies. Figures 3(a) and 3(b) show typical potential families for $^{10}\text{B} + ^{232}\text{Th}$ system at 65 MeV that give similar fits for the real and imaginary parts, respectively. At each beam energy, radii of sensitivity for both real and imaginary parts are determined. R_{sr} and R_{si} are obtained for all incident energies to be in the ranges of 11.2 to 12.4 fm and 10.9 to 15.8 fm, respectively, for the $^{10}\text{B} + ^{232}\text{Th}$ system and in the ranges of 11.3 to 12.4 fm and 12.3 to 16.4 fm, respectively, for the $^{11}\text{B} + ^{232}\text{Th}$ system. The average sensitive radii for the $^{10}\text{B} + ^{232}\text{Th}$ system for full energy range are $R_{sr} = 11.67$ fm and $R_{si} = 13.12$ fm and for $^{11}\text{B} + ^{232}\text{Th}$ system these values are $R_{sr} = 11.57$ fm and $R_{si} = 13.34$ fm. An average of R_{sr} and R_{si} was used in the dispersion relation as a effective sensitive radius R_s for both the systems. The R_s values for the $^{10}\text{B} + ^{232}\text{Th}$ and $^{11}\text{B} + ^{232}\text{Th}$ systems are 12.39 and 12.45 fm, respectively [28].

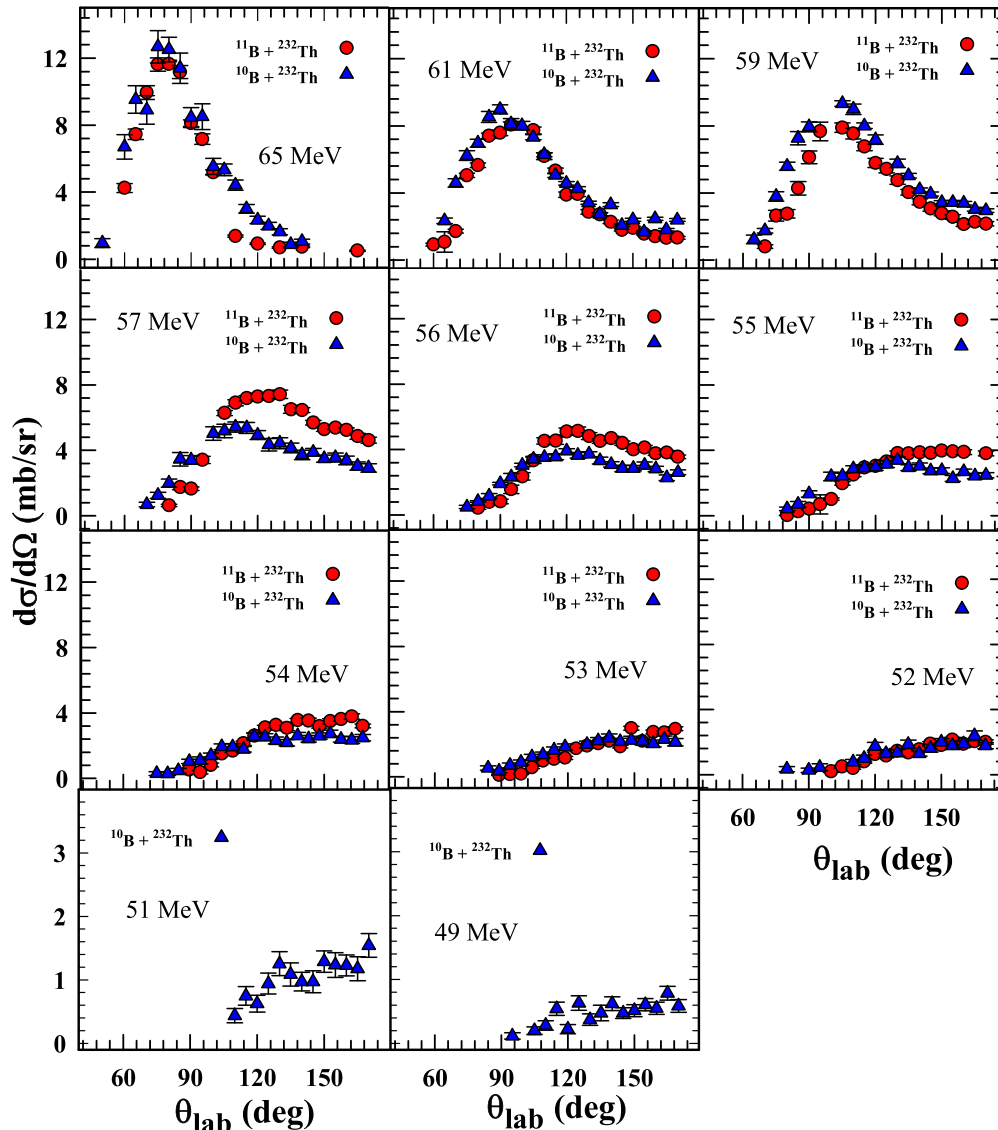


FIG. 5. Transfer angular distributions for $^{12,13}\text{C}$, $^{9,10}\text{Be}$, and $^{6,7}\text{Li}$ at various bombarding energies for $^{10,11}\text{B} + ^{232}\text{Th}$ systems.

The energy dependence of the real and imaginary optical model potential parameters (from Tables I and II) for $^{10,11}\text{B} + ^{232}\text{Th}$ systems are shown in Fig. 4. The error bars in this figure represent the range of deviation of the potential corresponding to χ^2 variation of one unit. It can be observed that with the decrease in beam energy, the imaginary potential decreases and the corresponding real potential increases at energies near the Coulomb barrier. The present behaviors of real and imaginary potentials are similar to the well-known characteristics for the usual threshold anomaly, which was observed earlier for tightly bound ^{12}C , ^{16}O projectiles [4,8,11].

The dispersion relation analysis was carried out using Eq. (1) to check the consistency of the optical potentials as a function of beam energy (E). Using the knowledge of empirical values of the optical model absorption term $W(E)$ at sensitive radius (R_s), Eq. (1) allows us to evaluate ΔV , the dispersive contribution to the real part. The analysis has been performed at each energy between 52 and 65 MeV for the $^{11}\text{B} + ^{232}\text{Th}$ system and between 49 and 65 MeV for the $^{10}\text{B} + ^{232}\text{Th}$ system. In order to get the real part through the dispersion relation, the linear segment model proposed in Ref. [30] was used in the imaginary part. Two sets of the real potential $V(E)$ were obtained by numerical integration of Eq. (1) using two different line segment (red and blue lines) fits of imaginary potential $W(E)$ [31]. The dispersion relation also exhibits a local peak in real potential with rapid decrease in imaginary potential at energies below the barrier as shown in the Figs. 4(a) to 4(d). This is clearly an indication of threshold anomaly in the $^{11}\text{B} + ^{232}\text{Th}$ system [Figs. 4(a) and 4(b)] as well as for the $^{10}\text{B} + ^{232}\text{Th}$ system [Figs. 4(c) and 4(d)]. Thus, the real and imaginary optical potential parameters are consistent with the dispersion relation around the Coulomb barrier and therefore threshold anomaly is unambiguously observed in both $^{10,11}\text{B} + ^{232}\text{Th}$ systems. However, much below the Coulomb barrier, the dispersion relation underpredicts the experimental value of $V(E)$.

IV. ANALYSIS OF THE TRANSFER ANGULAR DISTRIBUTION

For the analysis of angular distribution of the transfer reaction products, we have measured the yield of $^{12,13}\text{C}$, $^9,^{10}\text{Be}$, and $^6,^7\text{Li}$ at various angles for both $^{10,11}\text{B} + ^{232}\text{Th}$ systems. The same telescopes were used for the measurement of both quasi-elastic as well as transfer products and we have normalized the data at various angles with the yield of the monitor detectors. The transfer cross sections were obtained from the yield of the transfer products at various angles comparing with the calculated Rutherford scattering cross sections at forward angles. Figure 5 shows the transfer angular distribution data for both the systems, which includes $^{12,13}\text{C}$, $^9,^{10}\text{Be}$, and $^6,^7\text{Li}$ for different bombarding energies.

In the case of ^2H or ^3H transfer from $^{10,11}\text{B}$ respectively, the projectile-like fragment will be ^8Be and it will immediately break into two α particles [32]. In the present experimental setup, only one of the α particles could be detected in the telescope. Moreover, the α particles will have contributions from compound nucleus evaporation [32]. Thus, we have not included the contribution alpha channel in the determination

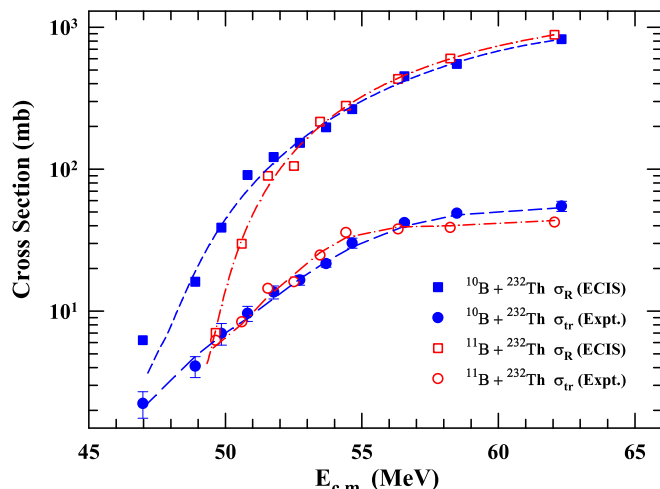


FIG. 6. Reaction cross sections for the $^{10}\text{B} + ^{232}\text{Th}$ system (solid square) and the $^{11}\text{B} + ^{232}\text{Th}$ system (open square) derived from fit to the quasi-elastic scattering angular distribution using the ECIS code. The transfer cross section (only sum of $^{12,13}\text{C}$, $^9,^{10}\text{Be}$, and $^6,^7\text{Li}$) are plotted for $^{10}\text{B} + ^{232}\text{Th}$ (solid circles) and for $^{11}\text{B} + ^{232}\text{Th}$ (open circles). Dashed and dash-dotted lines are guides to the eye.

of the transfer cross section. The transfer data overall show a bell-shaped angular distribution at above barrier energies as shown in Fig. 5. The grazing angle corresponding to the maximum yield shifts towards back angle with the reduction of the beam energy. The angle integrated transfer cross sections were calculated from the angular distribution data for different beam energies and are listed in Tables I and II for both $^{10,11}\text{B} + ^{232}\text{Th}$ systems.

In the present work, we have determined the reaction cross sections for both the systems from the fitting of the quasi-elastic angular distribution data. For comparison we have plotted both the transfer and reaction cross sections in Fig. 6. It is observed that the reaction cross section values for $^{10}\text{B} + ^{232}\text{Th}$ reaction are significantly large in comparison to $^{11}\text{B} + ^{232}\text{Th}$ at sub-barrier energies. This enhancement in the cross section may be due to the contribution of the breakup-fusion process for $^{10}\text{B} + ^{232}\text{Th}$ reaction, because of the relatively smaller breakup threshold of the ^{10}B projectile as compared to the ^{11}B projectile.

V. UNDERSTANDING OF REDUCED REACTION CROSS SECTION

In order to study the projectile effect for different systems, it is required to suppress the differences arising from the size and the charges of the systems. A reduction methodology proposed by Gomes *et al.* has been widely used for this type of study to understand the reaction mechanism [33]. In this method, the quantities $\sigma_R / (A_P^{1/3} + A_T^{1/3})^2$ vs $E_{c.m.} (A_P^{1/3} + A_T^{1/3}) / Z_P Z_T$ are plotted, where the subscripts P and T represent the projectile and target, respectively. Here, σ_R is the reaction cross section as plotted in Fig. 7(a). This analysis procedure has been successfully adopted in the past by several groups [3,19,28,29,34,35]. In the second method, the reduced reaction cross section $\sigma_R / \pi R_b^2$, is plotted as a function of the center of mass energy

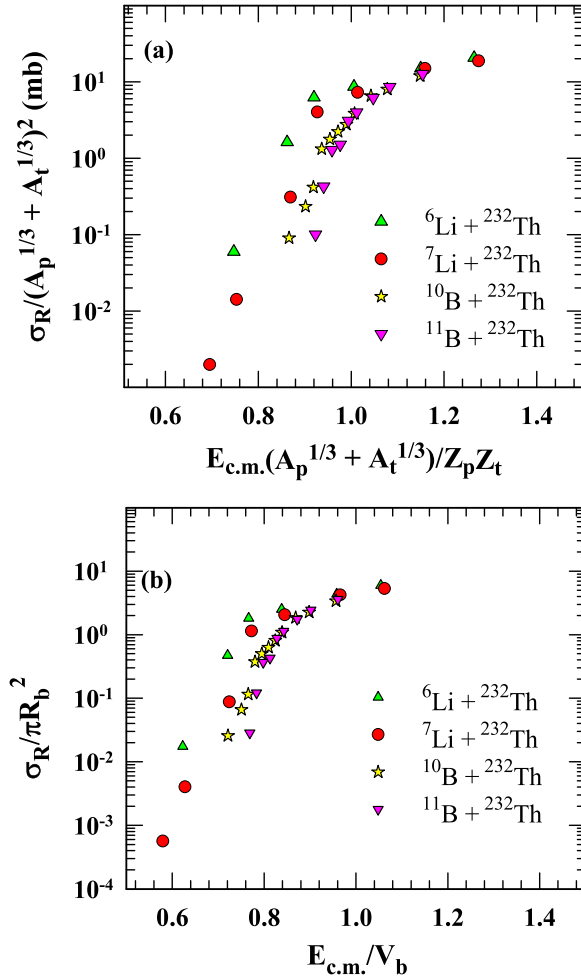


FIG. 7. Reduced reaction cross section for the $^{10,11}\text{B} + ^{232}\text{Th}$ systems compared with $^{6,7}\text{Li} + ^{232}\text{Th}$ systems [19] using the two reduction procedures (first taken from Refs. [19,33,36] and second taken from Ref. [36] as mentioned in the text).

normalized to barrier, $E_{c.m.}/V_b$ as shown in Fig. 7(b) [36]. It was suggested that the procedure removes the dependence on the charge and mass of the collision partners, but not on specific features of the projectile density, particularly when

weakly bound projectile nuclei are involved. Figure 7 shows a comparison of the reduced reaction cross sections for four different projectiles ($^{6,7}\text{Li}$ and $^{10,11}\text{B}$) interacting with ^{232}Th target. It is observed that the reaction cross sections are relatively large for weakly bound ^6Li and ^7Li projectiles, because of low ^4He -breakup threshold energy of ^6Li (1.48 MeV) and ^7Li (2.47 MeV) as compared to $^{10,11}\text{B}$ (4.46 and 8.66 MeV respectively). From the systematics for all the systems, it is found that at sub-barrier energies the reaction cross section gradually increases from ^{11}B to ^6Li , due to the reduction of the breakup threshold energy of the projectiles.

VI. SUMMARY AND CONCLUSIONS

In the present work we have carried out the simultaneous measurement of the quasi-elastic scattering and transfer angular distributions in $^{10,11}\text{B} + ^{232}\text{Th}$ systems for bombarding energies from 10% below to 20% above the Coulomb barrier. Optical model analysis of the experimental data have been performed to determine both the real and the imaginary parts of the optical potential as a function of beam energy. It is observed that as the bombarding energy decreases, the imaginary potential decreases and real potential increases. The behavior of the corresponding potential parameters as a function of energy is consistent with the usual threshold anomaly, confirming the tightly bound characteristics of both the projectiles, $^{10,11}\text{B}$. The reaction cross section obtained from the optical model analysis show large enhancement for the $^{10}\text{B} + ^{232}\text{Th}$ system in comparison to the $^{11}\text{B} + ^{232}\text{Th}$ system at sub-barrier energies. The reduced reaction cross sections have been obtained for both $^{10,11}\text{B} + ^{232}\text{Th}$ reactions and compared with the reactions of other projectiles ($^{6,7}\text{Li}$) with ^{232}Th target. The transfer products show a bell-shaped angular distribution at energies above the Coulomb barrier and the grazing angle shifts towards back angles at sub-barrier energies.

ACKNOWLEDGMENTS

The authors thank the operating staff of the BARC-TIFR Pelletron facility, Mumbai, for the excellent operation of the machine during the experiment. S.D. and S.M. acknowledge financial support from the UGC-DAE Consortium for Scientific Research, Kolkata Centre, India.

- [1] G. R. Satchler, *Phys. Rep.* **199**, 147 (1991).
- [2] A. G. Camacho, E. Aguilera, E. M. Quiroz, P. R. S. Gomes, J. Lubian, and L. F. Canto, *Nucl. Phys. A* **833**, 156 (2010).
- [3] D. Patel, S. Mukherjee, D. C. Biswas, B. K. Nayak, Y. K. Gupta, L. S. Danu, S. Santra, and E. T. Mirgule, *Phys. Rev. C* **91**, 054614 (2015).
- [4] M. A. Nagarajan, C. C. Mahaux, and G. R. Satchler, *Phys. Rev. Lett.* **54**, 1136 (1985).
- [5] A. M. M. Maciel, P. R. S. Gomes, J. Lubian, R. M. Anjos, R. Cabezas, G. M. Santos, C. Muri, S. B. Moraes, R. L. Neto, N. Added *et al.*, *Phys. Rev. C* **59**, 2103 (1999).
- [6] L. Fimiani, J. M. Figueira, G. V. Marti, J. E. Testoni, A. J. Pacheco, W. H. Z. Cardenas, A. Arazi, O. A. Capurro, M. A. Cardona, P. Carnelli *et al.*, *Phys. Rev. C* **86**, 044607 (2012).
- [7] N. Keeley, S. J. Bennett, N. M. Clarke, B. R. Fulton, G. Tungate, P. V. Drumm, M. A. Nagarajan, and J. S. Lilley, *Nucl. Phys. A* **571**, 326 (1994).
- [8] D. Abriola, A. A. Sonzogni, M. di Tada, A. Etchegoyen, M. C. Etchegoyen, J. O. F. Niello, S. Gil, A. O. Macchiavelli, A. J. Pacheco, R. Piegaiia *et al.*, *Phys. Rev. C* **46**, 244 (1992).
- [9] F. A. Souza, L. A. S. Leal, N. Carlin, M. G. Munhoz, R. Liguori Neto, M. M. de Moura, A. A. P. Suaide, E. M. Szanto, A. Szanto de Toledo, and J. Takahashi, *Phys. Rev. C* **75**, 044601 (2007).
- [10] D. Patel, S. Santra, S. Mukherjee, B. K. Nayak, P. K. Rath, V. V. Parkar, and R. K. Choudhury, *Pramana J. Phys.* **81**, 587 (2013).
- [11] P. Singh, S. Kailas, A. Chatterjee, S. S. Kerekatte, A. Navin, A. Nijasure, and B. John, *Nucl. Phys. A* **555**, 606 (1993).

- [12] B. R. Fulton, D. W. Banes, J. S. Lilley, M. A. Nagarajan, and I. J. Thompson, *Phys. Lett. B.* **162**, 55 (1985).
- [13] D. Abriola, D. DiGregorio, J. E. Testoni, A. Etchegoyen, M. C. Etchegoyen, J. O. F. Niello, A. M. J. Ferrero, S. Gil, A. O. Macchiavelli, A. J. Pacheco *et al.*, *Phys. Rev. C* **39**, 546 (1989).
- [14] A. Shrivastava, S. Kailas, P. Singh, A. Chatterjee, A. Navin, A. M. Samant, V. R. Raj, S. Mandal, and S. K. Datta, *Nucl. Phys. A* **635**, 411 (1998).
- [15] S. Y. Lee and W. Y. So, *Eur. Phys. J. A* **43**, 121 (2010).
- [16] P. R. S. Gomes, I. Padron, J. O. F. Niello, G. V. Marti, M. D. Rodriguez, O. A. Capurro, A. J. Pacheco, J. E. Testoni, A. Arazi, J. Lubian *et al.*, *J Phys. G* **31**, S1669 (2005).
- [17] M. S. Hussein, P. R. S. Gomes, J. Lubian, and L. C. Chamon, *Phys. Rev. C* **73**, 044610 (2006).
- [18] J. M. Figueira, J. O. F. Niello, A. Arazi, O. A. Capurro, P. Carnelli, L. Fimiani, G. V. Marti, D. M. Heimann, A. E. Negri, A. J. Pacheco *et al.*, *Phys. Rev. C* **81**, 024613 (2010).
- [19] S. Dubey, S. Mukherjee, D. C. Biswas, B. K. Nayak, D. Patel, G. K. Prajapati, Y. K. Gupta, B. N. Joshi, L. S. Danu, S. Mukhopadhyay *et al.*, *Phys. Rev. C* **89**, 014610 (2014).
- [20] A. Gómez Camacho, N. Yu, H. Q. Zhang, P. R. S. Gomes, H. M. Jia, J. Lubian, and C. J. Lin, *Phys. Rev. C* **91**, 044610 (2015).
- [21] Y. Y. Yang *et al.*, *Phys. Rev. C* **90**, 014606 (2014).
- [22] H. Leucker, K. Becker, K. Blatt, W. Korsch, W. Luck, H. G. Volk, D. Fick, R. Butsch, H. J. Jansch, H. Reich, and Z. Moroz, *Phys. Lett. B* **223**, 277 (1989).
- [23] D. C. Biswas, R. K. Choudhury, D. M. Nadkarni, and V. S. Ramamurthy, *Phys. Rev. C* **52**, R2827 (1995).
- [24] D. C. Biswas, P. Roy, Y. Gupta, B. N. Joshi, B. Nayak, L. Danu, B. V. John, R. Vind, N. Deshmukh, S. Mukherjee *et al.*, *J. Phys.: Conf. Ser.* **381**, 012091 (2012).
- [25] D. C. Biswas, R. K. Choudhury, B. K. Nayak, D. M. Nadkarni, and V. S. Ramamurthy, *Phys. Rev. C* **56**, 1926 (1997).
- [26] N. Majumdar, P. Bhattacharya, D. C. Biswas, R. K. Choudhury, D. M. Nadkarni, and A. Saxena, *Phys. Rev. Lett.* **77**, 5027 (1996).
- [27] J. Raynal, *Phys. Rev. C* **23**, 2571 (1981).
- [28] S. Dubey, S. Mukherjee, D. Patel, Y. K. Gupta, L. S. Danu, B. N. Joshi, G. K. Prajapati, S. Mukhopadhyay, B. V. John, B. K. Nayak *et al.*, *EPJ Web Conf.* **86**, 00008 (2015).
- [29] N. N. Deshmukh, S. Mukherjee, D. Patel, N. L. Singh, P. K. Rath, B. K. Nayak, D. C. Biswas, S. Santra, E. T. Mirgule, L. S. Danu *et al.*, *Phys. Rev. C* **83**, 024607 (2011).
- [30] C. Mahaux, H. Ngo, and G. R. Satchler, *Nucl. Phys. A* **449**, 354 (1986).
- [31] M. M. Gonzalez and M. E. Brandan, *Nucl. Phys. A* **693**, 603 (2001).
- [32] Y. K. Gupta, D. C. Biswas, Bency John, B. K. Nayak, A. Chatterjee, and R. K. Choudhury, *Phys. Rev. C* **86**, 014615 (2012).
- [33] P. R. S. Gomes, J. Lubian, I. Padron, and R. M. Anjos, *Phys. Rev. C* **71**, 017601 (2005).
- [34] N. N. Deshmukh, S. Mukherjee, B. Nayak, D. Biswas, S. Santra, E. Mirgule, S. Appannababu, D. Patel, A. Saxena, R. Choudhury *et al.*, *Eur. Phys. J. A* **47**, 118 (2011).
- [35] S. Mukherjee, N. N. Deshmukh, V. Guimaraes, J. Lubian, P. R. S. Gomes, A. Barioni, S. Appannababu, C. C. Lopes, E. N. Cardozo, and K. C. C. Pires, *Eur. Phys. J. A* **45**, 23 (2010).
- [36] C. S. Palshetkar, S. Santra, A. Chatterjee, K. Ramachandran, S. Thakur, S. K. Pandit, K. Mahata, A. Shrivastava, V. V. Parkar, and V. Nanal, *Phys. Rev. C* **82**, 044608 (2010).